Redox Biology 8 (2016) 383–397

Contents lists available at ScienceDirect

Redox Biology

journal homepage: www.elsevier.com/locate/redox

Research paper

CellNO trap: Novel device for quantitative, real-time, direct measurement of nitric oxide from cultured RAW 267.4 macrophages

Weilue He, Megan C. Frost *

Department of Biomedical Engineering, Michigan Technological University, 309 Minerals and Materials Building, 1400 Townsend Dr., Houghton, MI 49931-1295, United States

ARTICLE INFO

Article history:
Received 29 February 2016
Received in revised form
22 March 2016
Accepted 28 March 2016
Available online 31 March 2016

Keywords:
Real-time nitric oxide measurement
Adherent cell culture
Chemiluminescence

ABSTRACT

Nitric oxide (NO), is arguably one of the most important small signaling molecules in biological systems. It regulates various biological responses in both physiological and pathological conditions, often time producing seemingly contradictory results. The details of the effects of NO are highly dependent on the level of NO that cells experience and the temporal aspect of when and how long cells are exposed to NO. Herein, we present a novel measurement system (CellNO trap) that allows real-time NO measurement via chemiluminescence detection from general adhesive cultured cells using standard cell culture media and reagents that does not perturb the cells under investigation. Highly controlled light-initiated NO releasing polymer SNAP-PDMS was used to characterize and validate the quantitative data nature of the device. The NO generation profile from the macrophage cell-line RAW264.7 stimulated by 100 ng/ml LPS and 10 ng/ml IFN-γ was recorded. Measured maximum NO flux from RAW264.7 varied between around 2.5–9 pmol/10^6 cell/s under 100 ng/ml LPS and 10 ng/ml IFN-γ stimulation, and 24 h cumulative NO varied between 157 and 406 nmol/10^6cell depending on different culture conditions, indicating the conventional report of an average flux or maximum flux is not sufficient to represent the dynamic characters of NO. LPS and IFN-γ's synergistic effect to RAW264.7 NO generation was also directly observed with the CellNO trap. The real-time effect on the NO generation from RAW264.7 following the addition of arginine, nor-NOHA and L-NAME to the cultured cells is presented. There is great potential to further our understanding of the role NO plays in normal and pathological conditions clearly understanding the dynamic production of NO in response to different stimuli and conditions; use of CellNO trap makes it possible to quantitatively determine the precise NO release profile generated from cells in a continuous and real-time manner with chemiluminescence detection.

1. Introduction

Nitric oxide (NO), a gaseous molecule under STP (standard temperature and pressure), is a free radical solute that serves as a key signaling molecule in many cellular processes [1–7]. Nitric oxide has been shown to be a potent inhibitor of platelet adhesions and activation [8,9], plays a role in mediating the inflammatory process [10] and is an antibacterial agent [11]. It is well established as a neurotransmitter and plays a significant role in maintaining normal blood pressure [12]. NO has anti-apoptotic effects in endothelial cells, lymphoma cells, ovarian follicles, cardiac myocytes and hepatocytes [2]. Alternatively, NO has been shown to possess pro-apoptotic properties in macrophages, neurons, pancreatic β-cells, thymocytes chondrocytes and hepatocytes [3]. There are a number of reviews that suggest NO in low levels has a protective and proliferative effect on cells while at high levels induces cell cycle arrest, senescence and apoptosis [1,6,7]. The contradictory effects of NO are dependent in part on a number of factors including the flux of NO, the timing of NO release, and the type of cells exposed to NO. There has been a great deal of research in the past several decades dedicated to establishing an understanding the roles NO plays in this wide range of normal and pathological processes and attempting to harness the therapeutic potential of this molecule [13–21]. Despite these efforts and the huge potential of NO to affect cells, there are a lack of clinically relevant NO treatments available, owing largely to the difficulty in reconciling the wide variety and sometimes contradictory effects NO exerts on cells.

It is now clear that it is essential to understand both the amount of NO cells experience/generate as well as the temporal aspect of when cells experience/generate NO (this includes both the duration of NO as well as what point in the cell cycle NO is experienced). The measurement of NO in biological media has been the subject of several recent reviews [22–31]. It is well

* Corresponding author.
E-mail address: mcfrost@mtu.edu (M.C. Frost).

http://dx.doi.org/10.1016/j.redox.2016.03.006

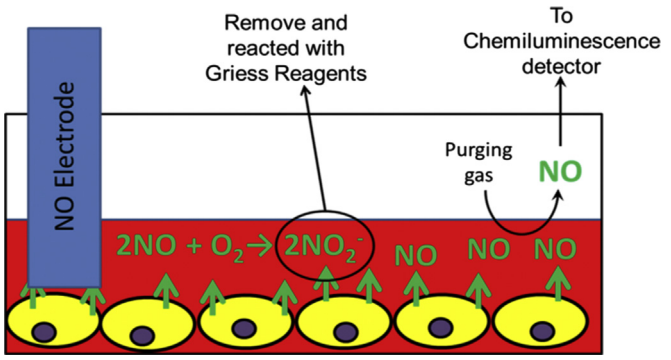

Fig. 1. Illustration of the 3 most common methods (an electrochemical sensor, the Griess assay for nitrite/nitrate, and gas phase chemiluminescence) for detection of NO in biological media.

established that this free radical signaling molecule is extremely difficult to measure owning to its high reactivity and diffusivity and the large number of biological molecules with which it will react. The half-life of NO is on the order of seconds to minutes in oxygenated solutions [32,33] and is substantially shorter in the presences of molecules such as hemoglobin and other free radicals [34–36]. Fig. 1 illustrates the three work horse methods utilized for measuring NO in biological solutions. They are the colorimetric Griess assay, which measures the accumulation of nitrite in aqueous solution resulting from the oxidation of NO [22,23,31], electrochemically by the oxidation of NO dissolved in aqueous solution [27,28], and with chemiluminescence detection of NO in the gas phase after its reaction with ozone [22,30]. Each of these methods has significant limitations in the quantitative measurement of NO from cells grown in culture. The Griess assay measures the accumulation of nitrite/nitrate over time and attributes the elevated levels of these ions to NO production. In a study to determine accuracy of this method with a standard NO donor, Hunter, et al. [22] reported that the Griess assay resulted in ~30% less total NO detected in phosphate buffered saline than the theoretical amount predicted by the concentration of the NO donor, PROLI/NO used. Different biological media that were also tested including serum, plasma, and DMEM, all showed an even greater variation was introduced. Importantly, the level of variation was also dependent on the total volume of solution used, making the bias in detection very difficult to calibrate. Electrochemical detection is a concentration based detection method and the results for quantitating the highly reactive NO molecule depend on a number of factors including distance of the electrode from the cells surface, trapping effect resulting from the size of the electrode, and stirring rate of the solution. Additionally, the electrodes can be very fragile and susceptible to fouling by biological molecules [37,38]. Chemiluminescence detection is based on the gas-phase reaction of NO with ozone to generate an excited state NO_2 molecule that relaxes to release a photon that can be counted [30,39,40]. This is a highly selective and sensitive method of detection but is limited by the need for NO to diffuse through culture media and enter the headspace above the cell culture dish and be swept into the chemiluminescence analyzer. The bathing solution in these experiments needs to be purged by a bubbling gas in order to force NO out of the solution phase before it reacts with species present in biological media. None of these techniques have provided satisfactory results for real-time determining the level of NO that cells produce or experience.

It has become abundantly clear that temporal aspects of NO release and under what circumstances it is produced, as well as what the duration of NO production that cells achieve are critical to understanding the roles NO plays in normal and pathological processes. As an example, Thomas and co-workers [41] demonstrated that the duration over which a dose of NO is delivered to cells has a profound impact on the protein expression of the cells. A single, large bolus dose of NO (average of 1000 nmol over 1 h) administered at time 0 showed increased production of $p5_3$-Ser-15, which indicated apoptosis. While a larger dose of NO delivered from time 0 and continued over a 9 h period (average of 400 nmol), showed a significant production of the anti-apoptotic factor HIF-1α. When the NO dose (average of 500 nmol over 9 h) was introduced later in the culture period, such that the maximum NO was experienced by the cells at 5 h, the ratio of HIF-1α and p53-Ser-15 was markedly different. This data clearly shows that the ultimate cellular fate may be affected by the amount of NO delivered and the timing of this delivery, highlighting the importance of understanding the temporal variable involved in when cells experience the NO as well as the duration over which a specific dose of NO is delivered.

Since both the dose and duration of NO have a profound impact on the ultimate cellular reaction to NO, understanding the level and the temporal variables of cell production of NO should greatly improve the design of NO releasing materials and delivery devices and accelerate the successful clinical application of this highly promising therapeutic molecule. Here in, we describe an easy and reliable method of directly measuring the flux of NO(g) from cultured living cells continuously in real-time fashion by chemiluminescence detection that overcomes the challenges of detecting NO within the culture medium. The design of our measurement device, called CellNO trap, was inspired by classical Boyden chamber co-culture system, which allows soluble signaling molecules to cross a porous membrane separating cell types (Fig. 2). While two different types of cells are cultured in two different chambers separated by a porous membrane, which could minimize direct cell-cell contact but allows soluble signaling molecules to passing through the partitioning membrane and cell-cell intertalk was achieved when the effective cells received the soluble signaling molecules (Fig. 2A). Similarly we created an NO measurement device composed of two chambers (Fig. 2B). The upper chamber is for conventional cell culture, and the lower chamber is used to sample gaseous NO diffused from cells. The ability of the CellNO trap to measure both the dose and the timing of NO generation was verified by using a photosensitive NO releasing material, S-nitroso-N-acetylpenicillimine modified polydimethylsiloxane (SNAP-PDMS), developed by our laboratory [42,43]. Macrophages (RAW-264.7) cells were cultured in the device and stimulated to demonstrate the ability to measure NO released from cells in a real-time, continuous manner. Additionally, retinal epithelial (ARPE-19) cells, mouse vascular smooth muscle (MOVAS) cells, vascular endothelial (SVEC) cells, L-929 cell and mouse primary tenocyte were tested in the CellNO trap to show general applicability of the device to multiple cell types.

2. Materials and methods

2.1 Cells and chemicals

RAW264.7 cell, ARPE-19 cell, MOVAS cell, SVEC, and fetal bovine serum (FBS), phosphate buffered saline (PBS), Dulbecco's modified eagle medium (DMEM) were all purchased from ATCC (Manassas, VA). L-929 cell and mouse primary tenocyte (kindly provided by Dr. Rupak Rajachar, Houghton, MI). Silanol-terminated PDMS, (3-aminopropyl) trimethoxylsilane, dibutyltin dilaurate were purchased from Gelest Inc. (Morrisville, PA). Room temperature vulcanized PDMS (RTV-3140) and silicone elastomer base and curing agent (Sylgard® 184) were acquired from Dow Corning Co. (Midland, MI). Interferon-γ mouse was obtained from BD

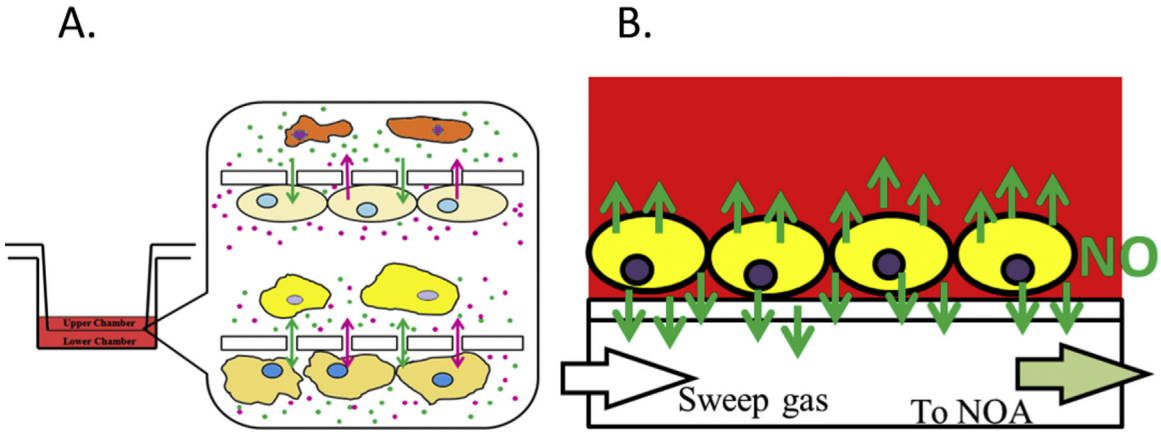

Fig. 2. Illustration of the principle of the CellNO trap, a novel NO measurement system. (A) The cell co-culture system Boyden chamber allows soluble cell excretion to diffuse between the two chambers, which are separated by the porous membrane. (B) The device is comprised of 2 chambers akin to the co-culture system, the upper chamber is where cells are cultured. NO produced by the cells diffuses in all directions, including crossing a gas-permeable, water-impermeable PDMS polymer layer that forms the bottom of the upper chamber. The lower chamber of the device serves as the gas sampling chamber from which cellular NO was detected via chemiluminescence by a continuous sweep gas.

Biosciences (San Diego, CA), lipopolysaccharine, L-arginine, N-acetyl-D, L-penicillamine, acetyl anhydrate, calcein-AM, and 4-amino-5-methylamino-2′,7′-difluorescein (DAF-FM), and cyclam were obtained from Sigma-Aldrich (St. Louis, MO). Tertbutyl nitrite was purchased from Acros Organics, (Pittsburgh, PA). Toluene was purchased from Mallinckrodt Chemicals (Phillipsburg, NJ). N^{ω}-hydroxy-nor-Arginine (nor-NOHA), L-N^{G}-Nitroarginine methyl ester, and nitrate/nitrite colorimetric assay kit were obtained from Cayman Chemical (Ann Arbor, MI). Gelatin was obtained from Bio-rad (Hercules, CA). Pyridine was purchased from EMD Chemical Inc. (Darmstadt, Germany). Ethidium bromide was obtained from Invitrogen (Grand Island, NY).

2.2 CellNO trap fabrication

Solutions of PDMS (either 1 g RTV-3140 dissolved in 10 ml of toluene or 0.5 g Sylgard® dissolved in 10 ml toluene) was manually cast on the top of glass fiber filter paper to form NO permeable and cell culture compatible membranes. Different thickness of PDMS membrane was achieved by casting multiple layers of PDMS

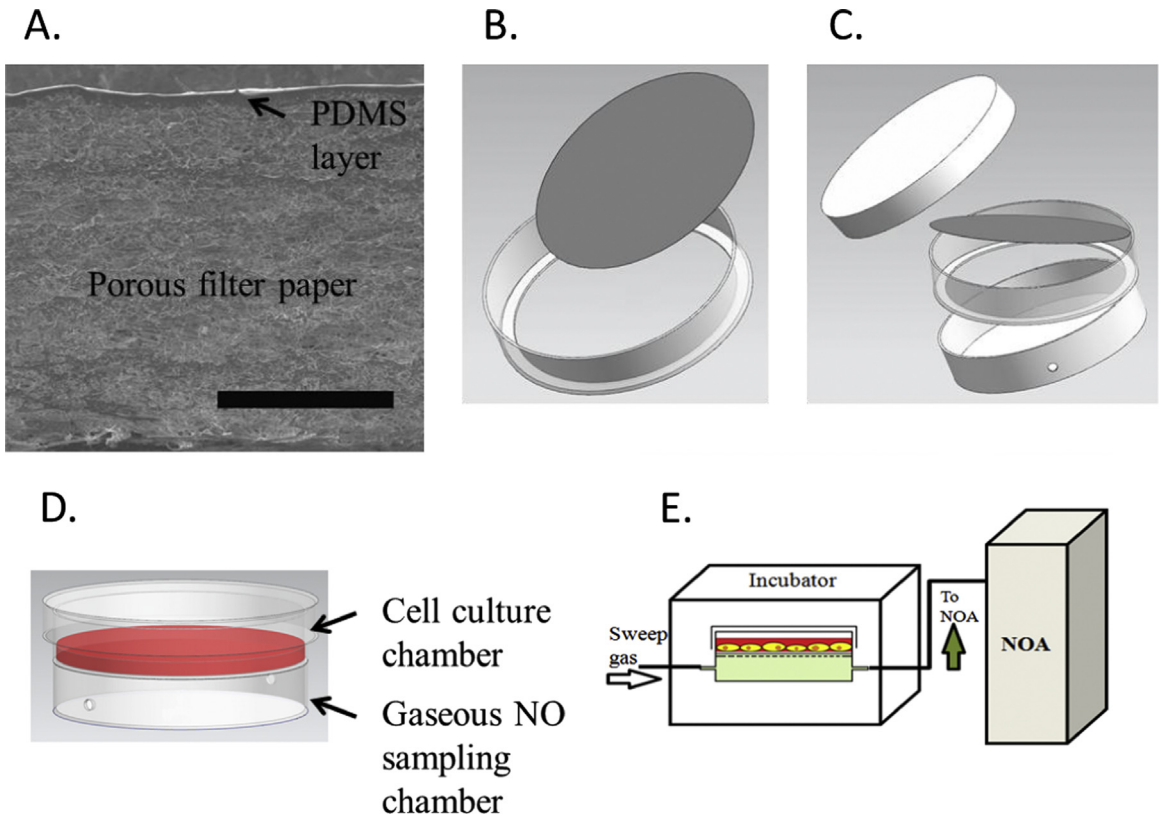

Fig. 3. Illustration of the construction of the CellNO trap. (A) SEM image of NO-permeable, water-impermeable membrane composed of micron thick polymer layer formed on top of glass fiber filter-paper, scale bar: 200 μm. (B) PDMS coated glass fiber filter paper was attached to a conventional polystyrene cell culture dish which had the bottom removed. The PDMS coated glass filter forms the bottom of the culture chamber. (C) The main components of a fully assembled device, including dish cover, selective-permeable membrane that separates the upper and lower chambers. (D) Cell culture experiment set-up in which cells were seeded within the upper chamber and the device was placed within cell incubator for normal cell culture and coupled to the sampling lines that attached to the chemiluminescence NO detector. (E) Illustration of how NO sampling can be initiated and stopped at any time point during cell culture according to specific experimental design.

solution on the filter paper. For cell culture, 3 layers of PDMS solution (either RTV-3140 or Sylgard®) were cast (72 μl/cm^2) onto the glass fiber filter paper and dried for overnight for complete curing. The bottom of 100 mm dia. × 20 mm deep or 60 mm dia. × 15 mm deep polystyrene cell culture dishes were removed, leaving a 2.5–3.5 mm wide rim around the bottom of the plate (Fig. 3A). The PDMS covered glass fiber filter paper was adhered to the culture dish, creating a PDMS/glass filter paper bottom (Fig. 3B). A second culture dish was attached under the PDMS-bottomed dish and two holes were drilled in the wall of the lower chamber, creating a cell culture dish with two chambers (Fig. 3C). Upper chamber was further top-coated with 2 mg/ml dopamine solution for 24 h (in 10 mM Tris buffer, pH = 8.5). The whole device was sterilized through ethylene oxide for 24 h and then the polydomapomine surface was treated with a 2 mg/ml gelatin solution for 1 h, after which the device is ready for cell culture (Fig. 3D). Device was placed within a cell culture incubator and the lower chamber was connected to the chemiluminescence NO analyzer sampling line for real-time continuous NO measurement (Fig. 3E).

2.3 SNAP-PDMS synthesis

The photo-sensitive NO releasing polymer SNAP-PDMS was synthesized according the previously published method [42,43]. Briefly, 1.6 g of 2000 cSt silanol-terminated PDMS were dissolved in 4 ml of toluene and mixed with 2 ml of 0.15 g/ml (3-aminopropyl) trimethoxysilane toluene solution. After vortex-mixing, 1.0 ml of dibutyltin dilaurate stock solution (1.25 mg dibutyltin dilaurate/ml of toluene) was added. The PDMS mixture was continually stirred at room temperature for 24 h to allow for cross-linking. Self-protected N-acetyl-DL-penicillamin thiolactone was synthesized according to the method developed by Moynihan and Robert [44]. Then 50 mg of the thiolactone, 1 ml of toluene, and 2 ml of the cross-linked PDMS solution were mixed together and stirred for another 24 h. The tethered thiol groups were then nitrosated with t-butyl nitrite. SNAP-PDMS solution and RTV-3140 solution was manually cast in Teflon molds in three alternating layers to form RTV-3140 encapsulated 200 μm thick SNAP-PDMS film. Polymer films were stored in the dark at 4 °C until use.

2.4 CellNO trap validation and calibration

Controllable light-initiated NO releasing polymer SNAP-PDMS was used to release NO at different surface fluxes by illuminating the films with variable levels of light from a 470 nm LED (VAOL-5GSBY4, Mouser electric, Mansfield, TX). NO flux was measured via chemiluminescence detection with a Sievers 280i Nitric Oxide Analyzer (NOA) (GE Instruments, Boulder, CO) using 200 ml/min flow rate, with both house nitrogen and ambient air as the sweep gases. The instrument was then calibrated with zero NO gas and 45 PPM calibration NO gas standard (Air Liquid Healthcare America Corp. Plumsteadville, PA). Nitrogen or ambient air was used as sweep gas to carry NO into the chemiluminescence analyzer for direct NO measurement. Deviations caused by different sweep gases (N_2 or ambient air) were evaluated via linear regression and student *t*-test. RTV-3140 coated SNAP-PDMS was placed within the upper chamber on the surface upon which cells were grown (Fig. 8A). Polymer was submerged with either PBS solution, or DMEM media, or no bathing solution. Signal response time and NO releasing rate were evaluated by simultaneously recording NO flux from the both upper and lower chambers of the measurement device with two identically calibrated NOAs.

2.5 Cell culture and treatment

Mouse macrophage cell line (RAW264.7) was kept in culture in conventional polystyrene petri-dish within complete DMEM (with 10% FBS and 1% penicillin-streptomycin). Cells were scraped off and reseeded into the upper chamber of the CellNO trap. RAW264.7 cultured within complete media was used as the negative control. Cells were stimulated with LPS and/or IFN-γ. During NO measurement, different reagents which may change cellular NO generation profile were administrated to cultured cells such that the final concentration of the reagents are specified, including arginine (an additional 1 mM), the arginase inhibitor nor-NOHA (10 μM), and the NOS inhibitor L-NAME (50 μM).

2.6 Direct measurement of NO release from cells

Cells were cultured within the CellNO trap using standard cell culturing conditions until confluent unless otherwise stated. RAW264.7 cells were then stimulated with LPS and/or IFN-γ. The CellNO trap device containing cells was then placed into 37 °C 5% CO_2 incubator. The lower chamber of the device was connected to NOA. Cellular NO generation was measured in PPB/sec (parts per billion/s) and was converted to moles/sec and normalized to surface area per time to determine the surface flux of NO released by the cell layer (nmole cm^{-2} min^{-1}).

2.7 Cellular NO probing by DAF

DAF-FM stain was dissolved in DMEM to the final concentration of 10 μM. The DAF-FM contained media was applied to cultured cells and incubated for 20 min at 37 °C with 5% CO_2. Media was removed and cells were washed twice with PBS; then submerged in PBS and imaged using either Zeiss AxioVert 200 M Apo Tome or Olympus BX51 fluorescent microscope.

2.8 Cell image by fluorescent microscope

Cells were stained with live-dead assay reagents, 2 μM calcein-AM and 2 μg/ml ethidium bromide, in DMEM solution for 10 min. Fluorescently labeled cells were imaged via Zeiss AxioVert 200 M Apo Tome fluorescent microscope or Olympus BX51 microscope.

2.9 Membrane SEM and AFM imaging

The prepared semi-permeable membrane was cross-sectioned into 0.5 × 0.5 cm pieces. Membrane was platinum coated (50 nm) and imaged with a Hitachi S-4700 FE-SEM. Polydopamine and gelatin treated membrane was cut into 0.5 × 0.5 cm pieces for topographic image by Veeco Dimension 3000 at. force microscope. The aluminum reflex coated cantilever (Tap300Al-G, Budgetsensors) was used with a resonance frequency of 300 kHz and a force constant of 40 N/m.

2.10 Ultimate NO products assay

Cell cultured media was collected and total NO production was measured based on the hypothesis that all NO generated by cell ultimately transfers to NO_3^- or NO_2^-. The Griess assay was applied according to the protocol provided by Cayman Chemical Inc. In brief, 40–80 μl samples were incubated with nitrate reductase for 2 h to transfer all NO_3^- to NO_2^-; then Griess reagents N-(1-naphthyl)ethylenediamine and sulfanilic acid were mixed at specified ratios; 100 μl of Griess reagent mixture was added to samples and reacted for 10 min; sample absorbance was read at 540 nm by microplate reader (BioTek Instrument, Winooski, VT); known concentration gradient of sodium nitrite/nitrate solution

dissolved within complete cell culture media or PBS was used to obtain calibration curve.

2.11 Statistical analysis

The data was analyzed by either student's *t*-test or one-way analysis of variance. All statistical assays were achieved through R programming unless specifically noted.

3. Results and discussion

3.1 Fabrication of the CellNO trap and characterization of PDMS membrane

The principle of the widely used cell co-culture Boyden chamber, which takes the advantage of molecule diffusion, was used as the inspiration for this device (Fig. 2A). In our system, a two-chamber structure was designed to allow cells to grow in the upper cell-culture chamber using conventional cell culturing media and reagents and, at the same time, sample gas phase NO in the lower chamber. Once cellular NO diffuses through the interface, NO can be carried by the sweep gas into the NOA for continuous, real-time measurement (Fig. 2B).

The key component of the CellNO trap is the water-tight, NO permeable membrane used to separate the culture chamber from the NO sampling chamber. To create the two independent chambers, the membrane at a minimum needs to be 1) highly permeable to NO, 2) water impermeable, 3) compatible with cell growth, and 4) able to be readily fabricated. Polydimethoxylsiloxane (PDMS) was used as the critical component of this membrane because it has a large NO diffusion coefficient (up to 3.0×10^{-5} cm^2/s) [45], is highly hydrophobic such that it is impermeable to water, can be modified to be biocompatible, and is easy to cast into any shape. PDMS was cast into layers up to 20 μm thick layer, so that NO may diffuses through the membrane within one second [32]. This ensured the NOA data directly reflected the real-time NO released from the cell layer. However, since the thin PDMS layer itself is not stiff enough to provide the mechanical support that cell culture requires, PDMS was cast over a glass fiber filter paper. So that the glass fiber paper provided the mechanical strength while the PDMS created a gas permeable, water-tight chamber to form a culturing chamber. After surface treatment by polydopamine and ECM gelatin solution, the PDMS surface was ready for cell culture.

To achieve real-time NO measurement, NO gas molecules need to pass through the membrane as fast as possible, so that it can be detected using chemiluminescence in real-time. Considering

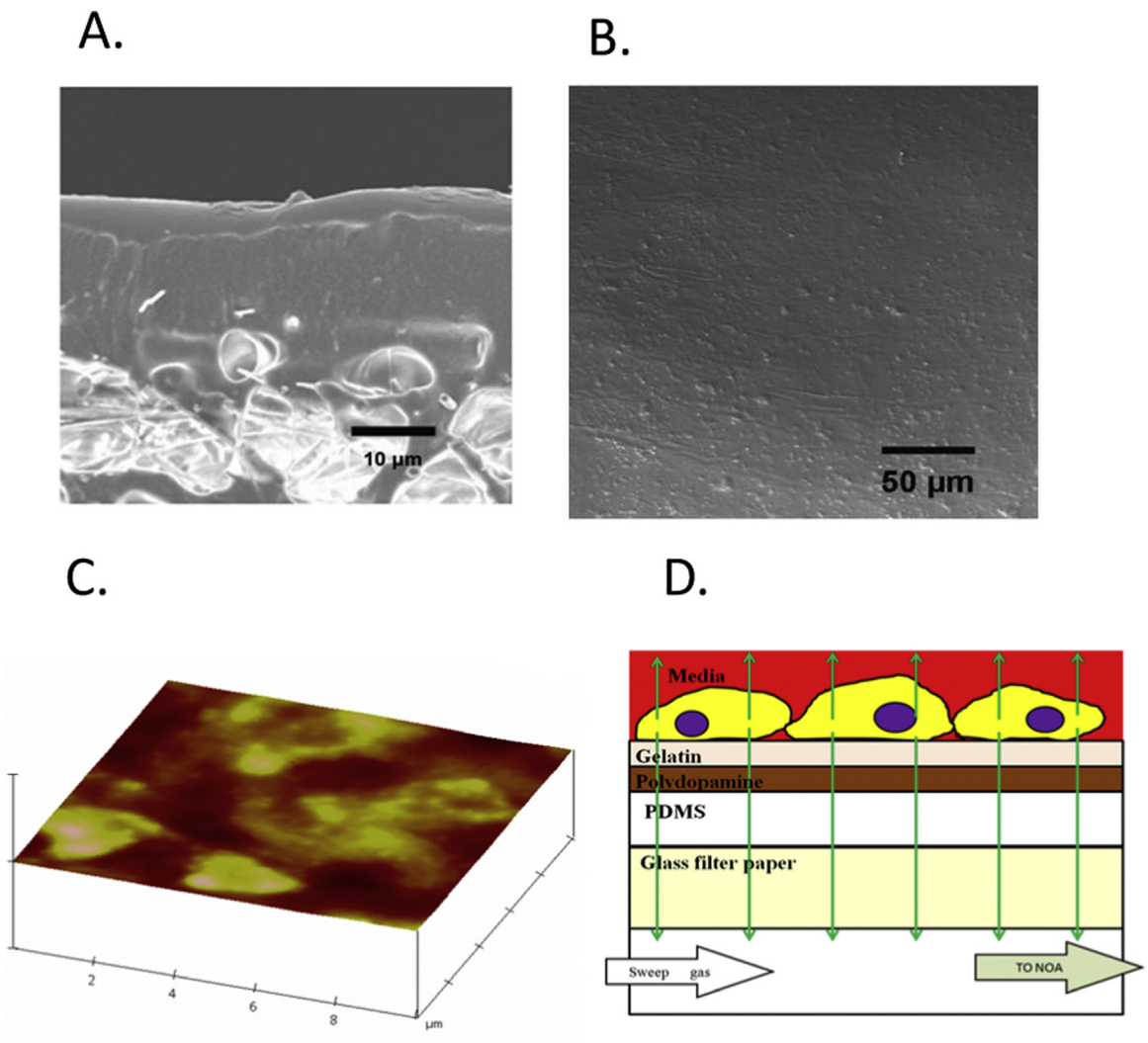

Fig. 4. Characterization of the membrane structure. (A) Cross-section of PDMS polymer layer by SEM; the polymer layer was 17.3 ± 3.2 μm thick according to SEM. (B) and (C) Topographic property of polydopamine and gelatin treated PDMS layer by SEM and AFM, respectively. AFM indicated the roughness (RMS) was 63.51 nm ± 19.60 nm. (D) Cells were cultured on polydopamine and gelatin top-treated PDMS layer; cellular NO diffused in all directions; once NO diffuses through PDMS layer into the lower chamber, NO was carried into NOA by sweep gas for surface flux measurement.

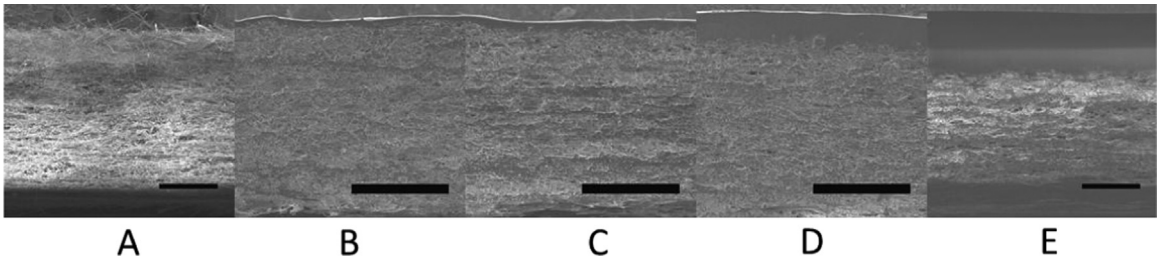

Fig. 5. Images that demonstrate the control over the thickness of the PDMS layer coated on the glass fiber filter paper. SEMs of different thickness of PDMS membrane by casting multiple layers of PDMS solution (for each cast, 72 μl/cm^2 solution was applied), scale bar: 150 μm. (A) glass fiber filter paper; (B) 3 repeat of 1 g/10 ml RTV-3140 cast; (C) 1 cast of 1 g/10 ml RTV-3140 and 2 repeat of 1 g/8 ml RTV-3140 cast; (D) 1 cast of 1 g/10 ml RTV-3140 and 3 repeat of 1 g/8 ml RTV-3140 cast; (*E*) 1 cast of 1 g/10 ml RTV-3140 and 4 repeats of 1 g/8 ml RTV-3140 cast.

Einstein–Smoluchowski equation, which describes the net molecule displacement, Δx, versus time (t) as

$$(\Delta x)^2 = 2Dt$$

where D represents the diffusion coefficient [32]. To get a small t value, a thin interface and large D are required. To achieve this, a diluted RTV-3140/Sylgard® solution in toluene was manually cast on glass fiber filter paper layer by layer with a total of 3 layers. Fig. 4A showed the cross-section of polymer coated glass fiber filter paper imaged by SEM. Total polymer thickness can be well controlled within 20 μm (17.3 ± 3.2 μm). To control and adjust the thickness of polymer layer, different concentration of RTV-3140 solution (0.1 g/ml and 0.125 mg/ml) and different number of layers cast can be used (Fig. 5). Since PDMS is not a good cell culture substrate, ECM component gelatin was used for surface treatment [46]. To do this PDMS was surface treated by coating with 2 mg/ml of dopamine first, which worked as intermediate adhesive, and further with 2 mg/ml gelatin solution applied over the polydopamine layer to assist cell adhesion for cell culture [46]. Fig. 4B and C showed the topographic images of the membrane by SEM and AFM, respectively. AFM quantified the surface roughness, root mean square (Rms) as 63.51 nm ± 19.60 nm, indicating a suitable surface roughness for cell culture [47]. Fig. 4D illustrates the structure of the final device with a cell culture chamber on top and gas sampling chamber at the bottom. The assembled device can be coupled to the chemiluminescence detector and placed within the incubator for measuring real-time NO released from cells (Fig. 3E).

3.2 Real-time measurement evaluation

To validate that real-time NO measurement can be achieved by sampling NO in the lower chamber of the device, a piece of the processed glass fiber membrane was fixed in between co-culture Kube® chambers; a 4 mm diameter, 0.1 mm thick SNAP-PDMS film was placed on the membrane in the upper chamber (Fig. 6); LED light was applied to the polymer to trigger NO releasing. SNAP-PDMS is a light sensitive NO leasing polymer, which releases NO at a highly controllable manner through changing the intensity of the light irradiating the polymer, and this response is linear [42] and is also demonstrated as shown in Fig. 7. Fig. 7A shows NO fluxing was controlled by changing the drive current applied to the LED, thereby changing the intensity of light produced by the LED. This property will be used later in the CellNO trap validation and calibration.

By sampling NO from both the upper and lower chambers using two identically calibrated chemiluminescence analyzers, the NO signal was simultaneously obtained from both chambers (Fig. 6). Once NO releasing was triggered by light, the NO flux was detected (first increase, in both blue and red lines) at the same time from both chambers, indicating no time delay of NO measurement across the membrane. Then the same light intensity was applied after PBS solution and DMEM media were added to the

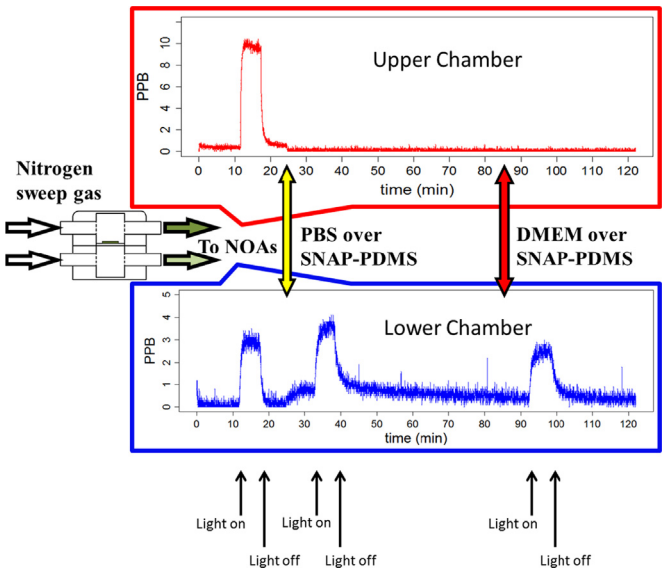

Fig. 6. Demonstration of the upper and lower chambers the ability to measure NO generated in the device. When bathing solution is added in the upper chamber, the NO signal is dampened but there is no impact on signal detected in the lower chamber. 4 mm diameter 200 μm thick SNAP-PDMS disc was placed on the PDMS coated filter paper, which separated Kube into two different chambers; LED light was used to photoinitiate controlled NO release from the SNAP-PDMS. Arrows indicate when the light was turned on and off. The NO surface flux from both upper and lower chambers was monitored by two identically calibrated NOAs at the same time. 100 μl PBS solution or DMEM cell culture media were applied onto SNAP-PDMS top one after another. The polymer interface was fully immersed by the bathing solution. (For interpretation of the references to color in this figure, the reader is referred to the web version of this article.)

upper chamber over the SNAP-PDMS disc with NO sampling continuing in both chambers. The addition of the bathing solutions dramatically hindered the gas phase measurement of NO flux in the upper chamber, while NO measured in the lower chamber remained relatively stable compared to the initial measurement with no bathing solution as the light was turned on and off (second and third increase in blue but not in red). Of particular importance, the NO measured in the bottom chamber showed release that exactly corresponded to the light being turned on and off, demonstrating that we maintained excellent temporal resolution for the tracking of the production of NO in the lower chamber, regardless of the addition of solution over the SNAP-PDMS disc in the upper chamber. This indicates that if we applied this system to cultured cells we should be able to record the temporal aspect cellular production of NO even when covered with culture media.

It should be noted that to prevent the potential oxygen tension reduction within cells by sweeping the lower chamber with pure nitrogen gas, ambient air (air drawn from within a 5% CO_2

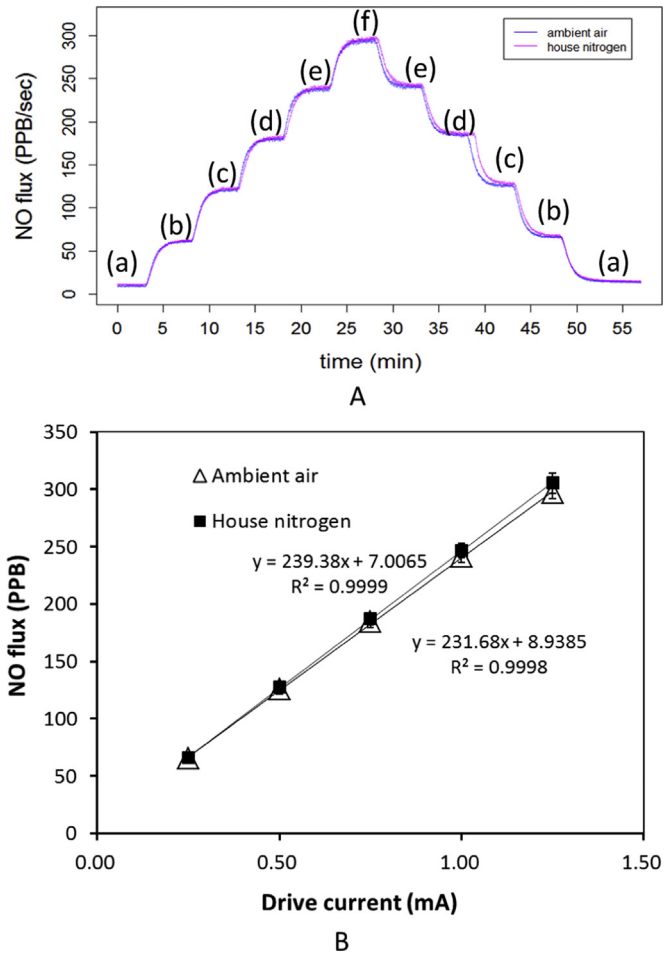

Fig. 7. Illustration of the effect of using ambient air as the sweep gas on the NO signal. 15 mm diameter, 0.2 mm thick RTV-3140 coated SNAP-PDMS was exposed under different LED light intensity by changing the LED drive current. House nitrogen and ambient air were used as sweep gases for independent experiments. (A) Representative curves of NO surface flux detected through nitrogen and ambient air by the same NOA. (a) to (f) represent 0.00 mA, 0.25 mA, 0.5 mA, 0.75 mA, 1.00 mA and 1.25 mA drive current, respectively. Three independent experiments were run. (B) Linear regression analysis of the NO flux vs. LED drive current by two different sweep gas. Though the slope values indicate around 3% loss of signal when ambient air is used as the sweep gas, paired student *t*-test applied to each value obtained at different drive current showed no statistically significant difference between the two groups.

incubator) was used as the sweep gas to carry NO into the NOA and zero calibration gas for the NOA in all subsequent experiments. To confirm that there was no significant difference between using house nitrogen and ambient air as the sweep gases, a control experiment was completed to evaluate the impact of the potential reaction of NO with oxygen present in ambient air during sampling. Fig. 7A shows the representative NO releasing profiles from SNAP-PDMS tested using both nitrogen and ambient air. No significant difference was found between the two profiles. Linear regression analysis showed linearity was good for both experimental conditions (R=0.9999 and 0.9998, while slope=239.38 PPB/mA and 231.68 PPB/mA for N_2 and ambient air, respectively); a slight decrease of detection sensitivity (slope in Fig. 7B, 3.2% decrease) was observed in ambient air group. This is an indication that there is a tendency of losing some NO signal by sampling with ambient air because of NO oxidation, however, by paired student *t*-test there is no statistically significant difference between the two groups (P=0.1926), indicating the feasibility of using ambient air and proper calibration to estimate cell NO generation.

3.3 Characterization of amount of NO detected by CellNO trap

The NO generated from cultured cell layer will diffuse in all directions, meaning in our system it will either enter media or diffuse through PDMS layer for sampling. The sampled NO should be only a part of the total NO generated by cells. Then we designed a series of experiments to find the relationship between the detected NO and the total amount of NO generated, aiming to use the gas sampled NO to quantify the total amount of NO generated.

To do this RTV-3140 coated SNAP-PDMS was used as NO source again; the polymer disc was attached tightly on the PDMS glass filter paper, membrane of the CellNO trap device, where different LED drive currents were used to adjust the rate of NO generation; NO was sampled in both upper and lower chambers (Fig. 8A). Total NO released was calculated as the sum of the total amount of NO generated from both upper and lower chambers, as determined by integrating the area under the NO release curves. Data showed clearly that the tested NO flux across the membrane (Fig. 8A blue line) changed in the same way as total NO flux changed (Fig. 8A, the sum of red and blue line). More importantly, after PBS was applied on top of NO source and the same LED drive current was repeated (same light energy to initiate the same NO release), NO flux through the membrane remained constant (Fig. 8A blue line after green arrow). However, the NO signal sampled from the upper chamber decreased dramatically (Fig. 8A red line after green arrow). This is expected since thick PBS bulk slowed NO diffusion such that NO auto-oxidation has more time to occur, which also explained why our device membrane needs to be thin. Linear regression analysis (Fig. 8B) further demonstrated that the bathing solution on top of NO source will not affect the NO flux into the lower chamber (Fig. 8B, blue slope remained after PBS addition), although it greatly decreased the detection sensitivity from the top chamber (Fig. 8B, red slope remained after PBS addition). It's also worth pointing out that although the signal detected in the upper chamber dramatically decreases, the NO production still increases linearly with increased LED drive current (Fig. 8B).

To ensure that CellNO trap maintained equivalent function for culture media, we changed the PBS bathing solution to normal complete DMEM, the same phenomenon was observed (Fig. 8C). Linear correlation of total NO generated (represented by the sum of NO detected from both chambers; upper chamber signal cannot be directly sampled at this point, so that media was collected and the Griess assay was applied to calculate the total NO generated) and the NO sampled from the bottom was examined (Fig. 8D). These results directly proved that the NO signal obtained from the lower chamber is linearly related to the total NO generation, indicating the feasibility of calculating total NO flux through simply multiplying NO flux detected from the lower chamber by an appropriate calibration factor.

3.4 Demonstration of cell compatibility with CellNO trap

RAW264.7 cells were seeded into both the NO measurement device and conventional 6-well cell culture plates with a starting seeding density of 10^5 cell/cm^2 for 24 h. Cell viability was evaluated by calcein-AM and ethidium bromide live-dead assay afterwards. No significant difference was observed in terms of total cell number and ratio of live and dead cells between those in the cell measurement device and conventional cell culture vessels by *t*-test (data not shown). After LPS stimulation, cell viability change was tracked through live-dead assay. Also no significant difference was found between the two groups (data not shown). To further test the cytocompatibility of the device, different cells including ARPE-19, MOVAS, L-929, SVEC, and mouse primary tenocyte were seeded at various seeding densities in the CellNO trap with different culturing time (up to 3 weeks). No cell toxicity was

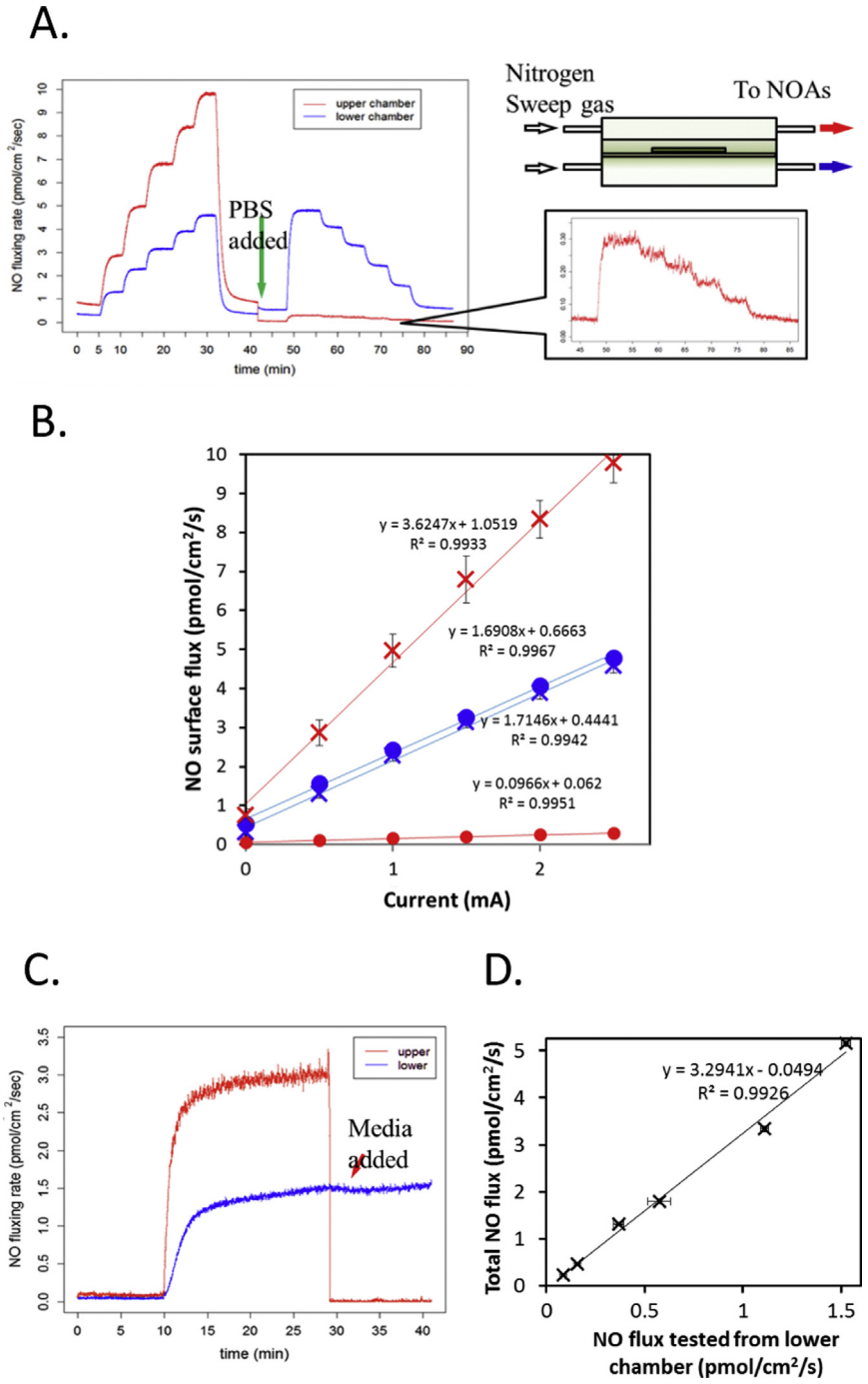

Fig. 8. Linearity of the detected NO signal over total NO generated in both gas-gas and gas-liquid chamber condition. (A) 15 mm diameter, 0.2 mm thick, RTV-3140 top-coated SNAP-PDMS was placed within NO measurement device. NO flux into both upper and lower chambers was tested by two identically calibrated NOAs simultaneously. Different NO flux was controlled by changing the drive current through a position fixed LED light. To assess the effect of bathing solution on top of NO source, PBS was applied and the same current intensity values were repeatedly applied. The damper of NO flux signal due to bathing solution was shown in the zoomed-in panel. Three independent experiments were run. (B) Linear regression analysis of results from (A). The slope reflects the detection sensitivity. Red refers to the signal from upper chamber, blue lower chamber; × corresponds to before adding bathing solution, • after. (C and D) Cell media was used as the bathing solution in the upper chamber. (D) Linearity test of the detected NO signal to the total NO while complete DMEM was used as the bathing solution. Media NO_2^- levels tested by Griess assay were used to estimate NO flux into the upper chamber and the total flux was represented by the sum of upper flux and lower flux. (For interpretation of the references to color in this figure legend, the reader is referred to the web version of this article.)

observed (data not shown). The purpose of using these different cell lines was to demonstrate that a wide variety of cells can be cultured within the device. Though no studies were completed to understand the role of NO in these varied cells, the utility of this device will allow detailed studies to be completed that will open the door to investigate how different cells respond to, produce and change the production of NO over time and under different stimuli conditions.

3.5 Measurement of real-time NO production from cells

The macrophage cell line RAW264.7 has be reported to produce NO at an average rate of 2.6 pmol/10^6cell/s under conditions of bacterial infection [48]. The Sievers 280i NOA utilized has a

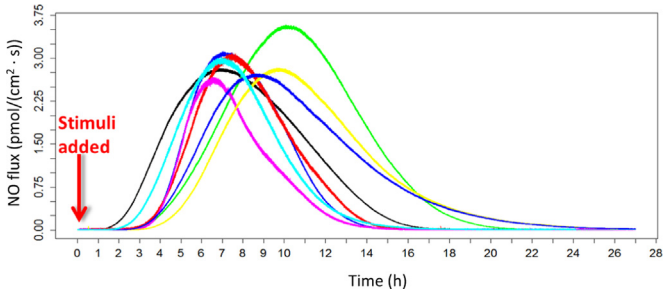

Fig. 9. Real-time NO release from macrophage cell-line RAW264.7 under 100 ng/ml LPS and 10 ng/ml IFN-γ combined stimulation. NO flux was normalized to dish surface area. (For interpretation of the references to color in this figure, the reader is referred to the web version of this article.)

calibration constant of around 0.1 pmol/PPB/s and should therefore have sufficient detection limit to monitor NO production in RAW264.7. RAW264.7 cells were cultured within the CellNO trap ($0.5–1 \times 10^6$ cell/cm^2) and stimulated with both 10 ng/ml IFN-γ and 100 ng/ml LPS. Immediately following stimulation, the device was connected to the NOA sampling inlet which was mounted in the cell culture incubator and connected to the NOA. Collection of continuous NO release lasted for series of time duration depending on applications (usually 17–48 h for RAW264.7).

Fig. 9 (each color represents one culture replicate) summarizes real-time NO releasing profiles, with similar peak shape, especially the time when maximum NO production occurred. Experimental data from the NOA was recorded as PPB/sec (volume ratio). After calibrating the NOA with acidified $NaNO_2$, an empirical calibration constant ranging from 0.8to 1.7×10^{-13} mol/PPB/s was obtained, depending on the specific flow rates, cell pressure, ozone reaction pressure and sweep gas used. Then PPB raw data can be converted to mol/sec, and NO surface flux can be quantified by normalizing to surface area of the culture (it is noted that this is not the surface

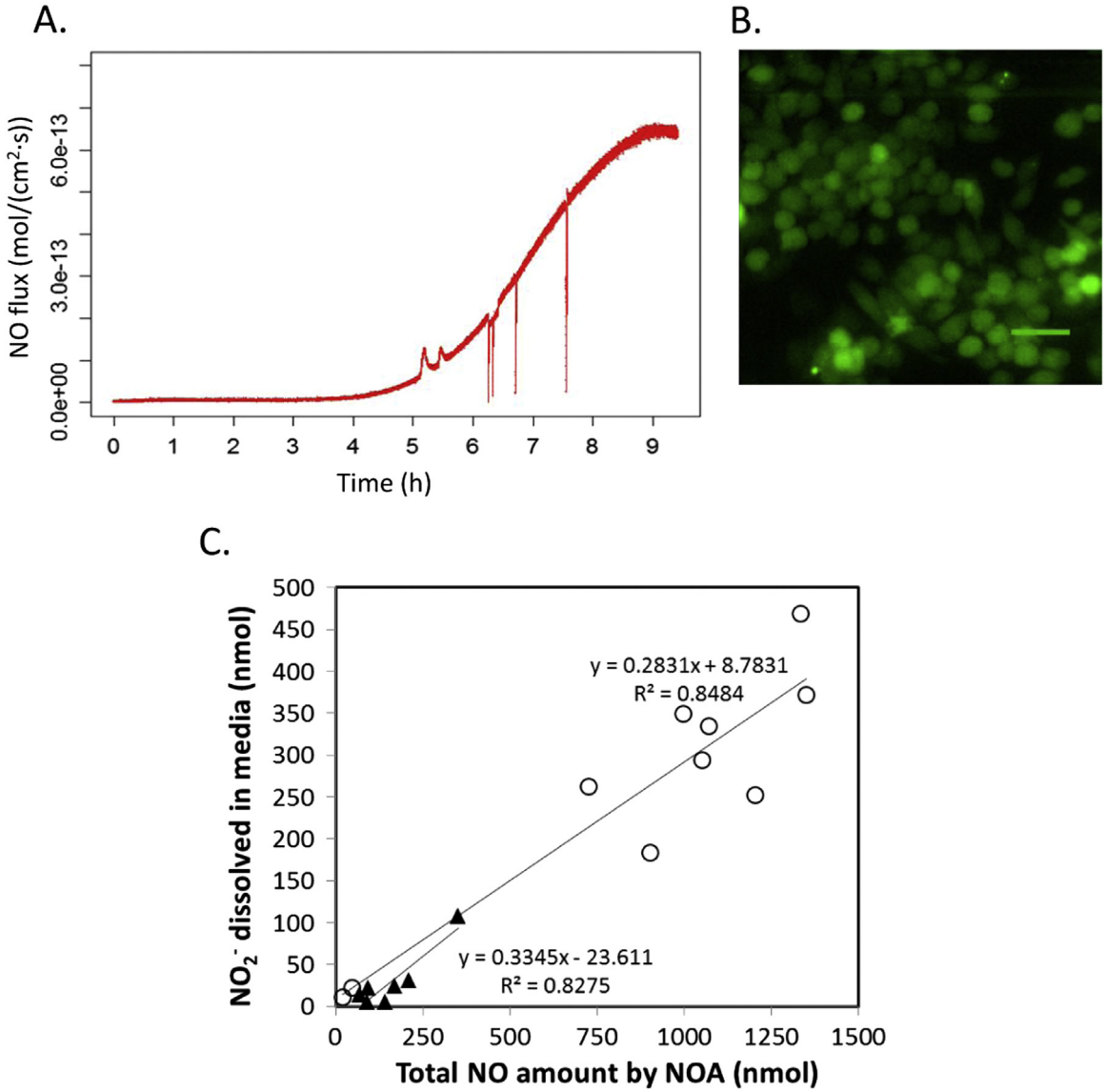

Fig. 10. NO release from RAW264.7 cells normalized to cell number. The NO release was measured by CellNO Trap (A), then NO positive cells were stained by DAF-FM (5 μM) and cell number was determined by fluorescent imaging, scale bar: 30 μm (B). Panel (C) illustrates the linearity of NO captured by the chemiluminescence detection and NO dissolved in media. RAW264.7 cells were stimulated by 100 ng/ml LPS and 10 ng/ml IFN-γ. NO penetrating the membrane was recorded by chemiluminescence detection. The total NO signal was calculated through integrating the area under the curve. NO dissolved and reacted within the media was determined using the Griess assay. Data points were plotted in the hollow circles. 35 μl of SNAP-PDMS solution was dissolved within 1 ml toluene and cast on to 60 mm NO measurement device and top-coated by 1 ml RTV-3140 solution, which generated around 25 μm (by calculation) thick polymer layer as NO source, which mimicked the cell layer and run the same experiment. Data were represented by the dark triangle.

area of the cells themselves, but is used as a reproducible and measureable approximation for the surface area). To evaluate the repeatability of this method, different sizes of device were also used for culturing cell. Normally the NO signal started to appear between 2 and 3 h. We cultured the cells within the device for 1–2 days to allow the cells to be confluent to form a relative uniform cell layer so that cell density could be relatively stable, normally ($0.5–1 \times 10^6$ cell/cm^2). 8 h after stimulation, cell death rate increased significantly according to live-dead assay (data not shown), which could be one of the reasons why the rate of NO production also decreased.

3.6 NO production normalized to cell number

To more precisely understand how much NO was produce by cells, we normalized the data to cell number. One of the drawbacks of our new cell measurement system is that although the cells can be observed through fluorescent labeling, the current membrane is not compatible with conventional visible light microscope. However, by fluorescent staining, the number of NO releasing cell can be determined and counted using fluorescence microscopy. After recording the NO releasing profile (Fig. 10A) from a specific culture, cells were removed from incubator and stained with the NO dye DAF-FM; then NO positive cells were counted under the microscope (Fig. 10B). By using the cell number to normalize the data, NO releasing from 10^6 cells was summarized in Table 1 Row 1 and 2. This number only represents NO detected from the lower chamber. To calculate the total NO released, culture media was collected from the upper chamber after NO sampling for analysis with the Griess assay. NO detected by the NOA using the CellNO trap and Griess assay from the media in the upper chamber of the device was presented in Fig. 10C (open circles). Overall, unlike the result in Fig. 8D, more NO (77.9%) appeared to be detected by the NOA, while 21.8% was trapped in the media (Fig. 8D showed a 23.4%: 76.5% ratio). We suspected that compared with cell layer (for RAW264.7, less than 15 μm thick), SNAP-PDMS film is normally much thicker (over 200 μm), the effect of a thicker film on the device membrane may influence the distribution of final NO diffusion (i.e., retarded diffusion into the lower chamber by effectively increasing the thickness of the membrane through which NO will diffuse). So we cast a thinner SNAP-PDMS layer (~25 μm) directly on the device and top coated with RTV-3140 to mimic cell generating NO from a thin cell layer. PBS solution was applied on top. The NOA recorded the NO flux in the lower chamber across the membrane and Griess assay tested the NO within the bathing solution. By analyzing the plot (Fig. 10C dark triangle), similar NO distribution to the cell culture experiment was observed (with 25.07% trapped in bathing solution and 74.93% NO went to NOA), proving the validity of our data and indicating that our method sampled the majority of NO generated by the cells. So the total NO generated by the cells should be presented as in Table 1 Row 3 and 4, which is consistent with the previous reports [48–50].

To verify the result obtained by this new method, we compared our method with the conventional NO measurement method Griess assay. RAW264.7 was cultured in both 6-well cell culture plate till confluent (around 10^7 cell/well) and our device (10.75 ± 0.65 cell/device). Then old media was removed and 2 ml of 100 ng/mlL LPS plus media were applied to the wells and 5 ml to the CellNO trap and connected to the NOA for real-time measurement. The accumulated NO generated was plotted in Fig. 11 (circles). For 6-well plate, samples of the media was collected at different time points and tested with the Griess assay. Fig. 11 solid squares show the time-dependent cumulative NO within the 100 ng/ml LPS stimulated media. Both results show a similar trend, that is before $t=4$ h, NO_2^- accumulation is mild (0.35 ± 0.51 nmol/10^6cell by Griess assay, 2.46 ± 0.12 nmol/10^6cell by NOA); there is a sharp increase of NO from 4 h to 11 h (to 17.23 ± 1.95 nmol/10^6cell by Griess assay and 30.23 ± 4.50 nmol/10^6cell by NOA); after 11 h, NO signal changed slowly, suggesting a slow-down of NO generation rate from 11 h to 16 h (to 17.51 ± 3.52 nmol/10^6cell by Griess assay and 33.30 ± 3.30 nmol/10^6cell by NOA), which suggests the time response of our method is reliable. However, the NO generation numbers determined according to the Griess assay were significantly lower (around 50% of our result) than the number measured by our method, which is also consistent with Hunter's report [22], indicating the significant problems associated with using the Griess assay to estimate the NO generation in practical biological applications and the much higher sensitivity of our methods.

Table 1
NO release from RAW264.7 cells stimulated by 100 ng/ml LPS and 10 ng/ml IFN-γ normalized to cell number (10^6 cells).

	Average	St.d.	95% Confidence area
AVG flux rate (pmole/10^6 cell/s)	1.73	0.63	1.73 ± 0.72
Max. flux rate (pmole/10^6 cell/s)	3.48	0.95	3.48 ± 1.08
Total NO (nmole/10^6 cell)	122.0	30.1	122.0 ± 34.8
Adjusted AVG flux rate (pmole/10^6 cell/s)	2.23	0.81	2.23 ± 0.92
Adjusted max. flux rate (pmole/10^6 cell/s)	4.47	1.22	4.47 ± 1.38
Adjusted total NO (nmole/10^6 cell)	156.6	43.8	156.6 ± 54.3

3.7 Investigation of temporal profile of NO production from RAW 264.7 cells

The dose-dependent biological effects of NO are beginning to be better understood, but we still lack data that shows how the temporal effect of NO plays a significant role in determining the ultimate biological response. Here we demonstrate three examples showing how utilizing CellNO trap can help understand the timing of NO generation.

IFN-γ and LPS can stimulate NO in a synergetic manner because the total accumulation of NO end-products is greater when both agents are used [51]. Fig. 12A shows the real-time NO releasing profiles from the same batch of RAW264.7 stimulated by 10 ng/ml IFN-γ alone, 100 ng/ml LPS alone, and both added at time zero. Fig. 12B–D focus on the initial stage of NO profile after stimulation, showing that in all the groups, NO generation started at around 2 h after stimulation, indicating that both pathways need at least

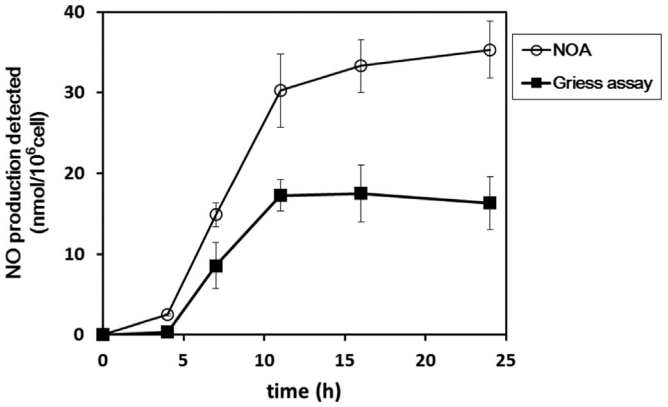

Fig. 11. Synergetic effect of LPS and IFN-γ to RAW264.7 NO generation. NO flux was normalized to surface area. (A) Representative profiles of RAW264.7 NO releasing under different stimuli. 100 ng/ml LPS, 10 ng/ml IFN-γ or a combination of the two were applied to stimulate the cells. The experiment and analysis were run by groups. The same group indicates the same cell passage, seeding density, prepared PDMS-coated filter paper and culturing time. (B)–(D) larger culture dishes (100 mm) were used to increase the magnitude of detected signal, showing the time point when NO signal starts to be detectable is nearly identical among groups.

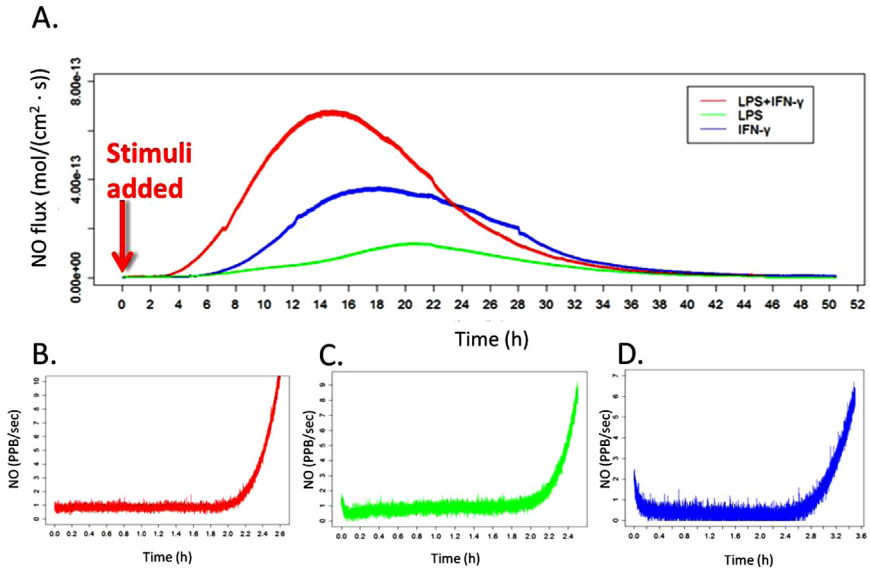

Fig. 12. The real-time NO releasing profile of RAW264.7 cultured under low cell density. Cells were cultured within the NO measurement device (60 mm diameter) to a final density of $1.61 \pm 0.24 \times 10^6$ cell/dish. Cells were stimulated by 100 ng/ml LPS and 10 ng/ml IFN-γ at time zero.

2 h to respond the stimuli to produce NO (the NOA has a detection limit of 0.5 PPB, a 1 PPB increasing of the average rate was considered to be the start of cellular NO generation; no significant difference among groups in regards to time required to initiate NO production was observed). Our method clearly showed how soon the stimulated cells begin to produce NO, the rate of NO production, the maximum level of NO produced by each stimuli individually and how long the NO production persists under static culture condition (without media change after treatment). IFN-γ and LPS alone initiated NO production with maximal surface flux of NO reaching 2.4×10^{-11} mol cm^{-2} min^{-1} after 18 h and 1.2×10^{-11} mol cm^{-2} min^{-1} after 22 h, respectively (measured value from the lower chamber only). When the same amount of IFN-γ and LPS were added together, NO production reached a maximal surface flux of 4.2×10^{-11} mol cm^{-2} min^{-1} (measured value from lower chamber) after only 15 h. Real-time, experimental data directly showed the increase in NO production when LPS and IFN-γ are added together is greater than either of them used separately. Integrating the area of the NO release curves allows the total dose of NO released to be calculated. Table 2 summarizes the integrated data from the NO releasing curve, Row 1–3. Compared with Noda's report [51], these numbers are far smaller (200 nmol/10^6 cell and 50 nmol/10^6 cell for LPS with and without IFN-γ respectively in their report). Cell viability tests indicated that in our system cells started to die at a high rate after 8 h of stimulation; the pH indicator in cell media also showed pH changed greatly between 8 and 12 h after stimulation. We suspected that in our system, the cell number might be too high compared with other models, which suppressed NO generation and affected cell behavior. So next, we reduced cell density and repeated the same experiment.

Fig. 13 showed that using the same stimulants (10 ng/ml IFN-γ and 100 ng/ml LPS at time zero) with a lower cell density ($1.24 \pm 0.18 \times 10^5$ cell/cm^2 compared to $5.56 \pm 0.33 \times 10^5$ cell/cm^2), NO release profile can be greatly altered. Compared with results in Fig. 9, NO signal also started between 2 and 3 h, but the NO releasing profile was elongated. Additionally, the rate of NO generation continued to increasing until up to 18 h (red). Compared with the high cell density groups (Fig. 9), NO flux normalized to cell number in the low density groups was significantly increased and the total NO generated (by integrating area underneath the curve from 0 to 24 h) also increased greatly (summarized in Table 2), showing how flexible NO production can be due to one simple factor such as different cell density. These number are two times larger than Noda et al.'s report [51] but in the same order of magnitude. This might be one of the reasons why there were significant variations in NO generation rate reported by different

Table 2
Result from the integration of the area under the NO release curve with different stimuli. NO release was normalized to cell number (106 cells). One way ANOVA and Tukey's test were performed with "*" denotes $P < 0.05$, compared with all the rest groups. "Δ" denotes P is approximately 0.2, compared with all the other groups. Other groups did not show statistically significant difference.

	Total NO release (nmol/10^6 cell)	**Std.**
100 ng/ml LPS	35.37	2.90
10 ng/ml IFN-γ	30.29	14.43
100 ng/ml LPS + 10 ng/ml IFN-γ Δ	156.6	43.8
100 ng/ml LPS + 10 ng/ml IFN-γ)*	405.57	54.67
100 ng/ml LPS + Arg at 4 h Δ	199.38	63.10
100 ng/ml LPS + Arg at 8 h	63.10	17.28
100 ng/ml LPS + Arg at 12 h	70.30	22.71
100 ng/ml LPS + nor-NOHA at 8 h	45.20	8.41
100 ng/ml LPS + L-NAME at 8 h	33.57	2.51

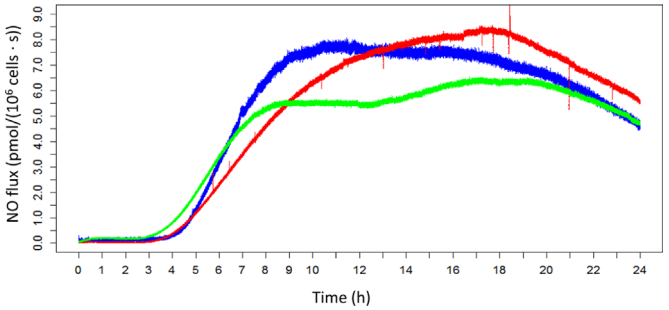

Fig. 13. Cumulative NO generated by cultured RAW264.7 measured by Griess assay and NOA. Cells were cultured within 6-well plate to the cell density of 10^7 cells/well. Two ml of 100 ng/ml LPS added media was applied to each well. Media sample was collected at times 0 h, 4 h, 7 h, 11 h, 16 h and 24 h. Three independent experiments were run. Samples were applied to Griess assay. To obtain the cumulative NO production by NOA, NO time-flux curves from NOA were applied to integration from 0 h to the correlated time points; then the membrane calibration constant was applied. Three independent experiments were run in triplicate.

groups. Cellular NO production rate can be very sensitive to cell environment. This highlights the importance of real-time measurement of every experiment and controlling the culturing conditions to obtain consistent results in NO generation from these cells otherwise results from different replicates or methods are not comparable.

Since arginine is the most important substrate for NO generation, we examined the relationship between NO generation and the arginine pathways. In RAW264.7 in vitro cultures, high doses of NO were produced, consuming large amount of Arg. Also, as a competing pathway, arginase catalyzes the urea cycle reaction which consumes arginine to form urea [52], thereby shunting arginine away from the NO production pathway. The arginine concentration might be an important limiting factor for NO production. In our study, exogenous arginine (an additional 1 mM) was added, the arginase specific inhibitor nor-NOHA (20 μM), and iNOS inhibitor L-NAME (50 μM) were added to 100 ng/ml LPS stimulated RAW264.7 cells (high cell density model was used here, $0.5–0.7 \times 10^6$ cell cm^{-2}).

One advantage of the two-chamber CellNO trap system is that the cell culture and NO measurement can be carried out independently but simultaneously. Treating cells and sampling can be processed simultaneously without generating confusing noise, so that the NO generation change introduced by condition changes can be tracked in real-time as well. After RAW267.4 cells were stimulated with 100 ng/ml of LPS and applied to the real-time NO measurement system, arginine was added at different time points into the cell culture media. Fig. 14A–C show that, right after Arg addition, the rate of NO production underwent a sharp increase. Considering time as a factor, the degree of increase in NO production upon the addition of Arg was significantly different at different time point of stimulation. When arginine was added at 4.5 h after stimulation, NO production increased slightly from 0.46 to 0.57 pmol/10^6 cell/s (Fig. 14A, by $28.9 \pm 4.1\%$ on triplicates average), however, after 8 h and 12 h, NO production increased by $85.2 \pm 2.3\%$ and $97.6 \pm 7.5\%$ on average, respectively (from 2.16 to

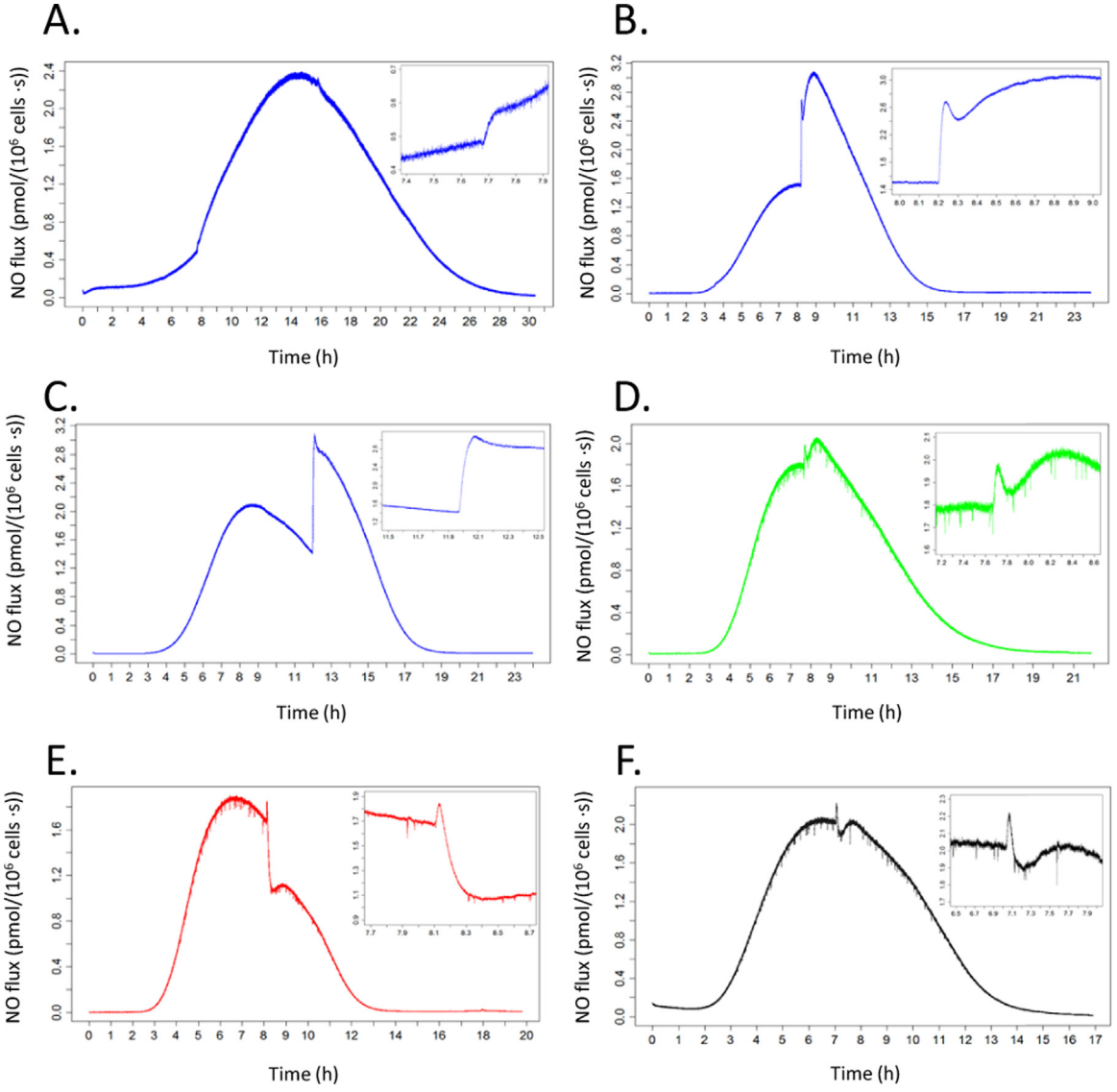

Fig. 14. Total NO generation from RAW264.7 cells stimulated with 100 ng/ml LPS monitored by chemiluminescence after the addition of different chemical agents that effect NO production. The curves at the up-right corner of each plot are expanded plots focusing on the change. (A)–(C) 500 mM Arg stock solution was added into media at different time point during cell culturing (resulting in a final concentration of 1 mM exogenous Arg in the culture media). (D) Arginase specific inhibitor nor-NOHA (final concentration of 20 μM) was applied to culturing media. (E) NOS inhibitor L-NAME (final concentration of 50 μM) was applied to the culturing media. To allow a homogenous distribution of the chemicals, device was gently shaken after chemical addition. To eliminate the possibility that the procedure itself may alter NO production, control (F) was run by adding PBS and shaking device gently. Total NO released by the cells was calculated by direct NO flux measured via chemiluminescence divided by the empirically determined membrane calibration factor of 77.9%.

4.37 pmol/10^6 cell/s and from 1.12 to 2.37 pmol/10^6 cell/s, in Fig. 14B and C). This could be explained by different limiting factors that occurred relative to different points of stimulation. With the consumption of Arg in static culture, after 8 h, the concentration of Arg might become the main limiting factor. So replenishing the Arg substrate for NO production might significantly change the NO producing profile. While at the initial stage, the amount of iNOS present might be the limiting factor. To further directly show that arginine accessibility determines NO production rate can be easily observed by our device, arginase specific inhibitor nor-NOHA, (which may potentially make more arginine accessible for iNOS), was applied. Fig. 14D shows 20 μM of nor-NOHA was applied to RAW264.7 after 8 h of stimulation, the NO production rate was increased from 1.99 to 2.30 pmol/10^6 cell/s (on triplicate average by 13.6 ± 4.0%), but not as potent as supplying arginine, which is around 1 fold. L-NAME's hydrolysis product inhibits NO production by binding with iNOS with high affinity. Fig. 14F showed that after supplying 50 μM of L-NAME, NO production indeed decrease from 1.68 to 1.07 pmol/10^6 cell/s (on triplicate average by 34.9 ± 4.0%) within 20 min (see Table 2). The total NO releasing after 24 h stimulation was summarized in Table 2. Noda et al. [51] reported the 24 h iNOS expression pattern after stimulating RAW264.7 by 100 ng/ml LPS using Western blot. The earliest immunoblotting band was characterized at 4 h. But it was not clear whether there was actual NO production within the initial 4 h after LPS stimulation due to their detection method and detection limits. We showed here that the NO signal appeared 2 h after stimulation. Using the CellNO trap system, we were able to directly measure both how much NO was produced and what the real-time level of NO production was. It is outside the scope of this work to complete the detailed molecular biology to fully determine the factors that are responsible for the changes in NO production when arginine is added and arginase and iNOS inhibited, but this devise will allow the molecular biology to be linked to direct NO detection and measurement, permitting the temporal aspect of NO release to be investigated.

Nitric oxide has multiple biological functions, which may be both deleterious and benevolent. The ultimate biological effects of nitric oxide might depend on a lot of parameters, including NO concentration, duration, and NO responding mechanisms within individual cells. Many of the contradictory roles that NO has been reported to play may be in part rooted in different temporal NO generation profiles caused by variable environmental conditions (e.g., different cell densities). But because of the lack of knowledge regarding the dose and duration of NO cells experience, attempting to understand the roles NO plays is complicated. Although attempts have been made to quantitatively determine the level of NO produced by cells or that cells experience, the problem remains unsolved because of the drawbacks within the measurement methods themselves. Western blot directly shows status of NOS isoforms, which have been used to indirectly indicate an increase or decrease in overall NO production. But this cannot be carried out in real-time or non-invasively and the actual NO level can be greatly affected by various things such as Ca^{2+} level (for nNOS and eNOS), cofactors, NO consumption rate, competitive reactions and levels of substrates and inhibitors. Immunohistochemitry or immunocytochemistry reveals NOS subcellular localization, which may be indicative and interesting in suggesting NO production, but in fact does not directly represent the level or NO production or the rate or for what duration NO is actually generated. NO fluorescent dyes such as DAF can hardly reflect NO real-time status and most NO dyes reflect NO accumulation in subcellular localization based on solubility and structures of the dyes. More importantly, the activation of the fluorescence signal is not actually dependent on NO but NO^+ equivalents, the oxidation products of NO, which makes this detection method less specific. Other indirect methods such as the Griess assay measures oxidized products, which is very likely to underestimate the amount of NO produced due to the escape of NO into cell culture head-space and reactions with other biomolecules (Deen's data [47]. shown in our data too). Directly measuring NO helps understand its biochemistry. The formation of other nitrogen oxides, which may be recognized as the NO signal by many current measurement methods, may cause the underestimation of the efficacy of NO by diminish the net NO level [36]. NO electrochemical microprobes have been used to record NO concentration measurement and can achieve real-time measurement but there is a great deal of variability in results when using probes of different sizes and results are heavily influenced by how close the probe is placed to the actual surface of cells under investigation [27].

By using the principle of Boyden co-culture chamber and high sensitivity of chemiluminescence NO analyzer, we fabricated a two-chamber, real-time cellular NO measurement device called CellNO trap. We emphasized here that to analyze biological samples, it's not enough to merely enhance limit of detection or increase data processing rate. Developing a biology-friendly interface is equally important, which brings about the minimum changes to the existing experimental protocols and introduces the least perturbation to biological systems. Our goal is trying to standardize NO data presentation, derive as much information as possible from the test systems and make NO data from different labs comparable.

Because of different requirements by specific applications, some limitations of the CellNO trap system need to be pointed out herein. This method does not directly provide concentration information, which can be estimated by calculation according to (ref). The current device is only applicable for in vitro cell culture system. One on-going research effort in our laboratory is to modify the device for measuring NO generation from tissues. This method investigates NO generation rate from significant amount of cells, and the result represents the average, not NO generated by one specific cell or local NO concentration. The limit of detection is mainly dependent on the sensitivity of NOA. To further improving the limit of detection is not easy. The method investigates each sample at a time, which makes less efficient compared to other methods that rely on the high-throughput microplate reader. But another on-going research project in our laboratory is trying to overcome this problem by designing new cell culture and sampling devices based on multi-well tissue culture plates.

In our system, due to the biocompatibility and gas-permeability of PDMS based substrate, cells were able to be seeded, grown, and tested in the same device without deviating from standard cell culture protocols. Dissolved NO was guided into gaseous phase and the flux was directly recorded. This only relies on the correct calibration of the instrument and the device. Some pioneers' work reported NO generation rate in cytokine/LPS stimulated RAW264.7. Normally the calculation is based on monitoring the change in NO concentration and, no other NO consumption routes other than certain specified chemical reactions [48–50]. The range differed from 2.6 ± 0.1 pmol/10^6 cell/s to 6.0 ± 0.4 pmol/10^6 cell/s, which is compatible with but generally a little less than our result. One reason could be the equations only considered the oxidation of NO by oxygen and superoxide, while in fact there are additional side reactions that potentially affect the NO consumption too.

Wang et al. mentioned NO oxidation in the PDMS membrane of their NO deliver system [53], which potentially could be one source of NO loss in our system too. However, their membrane was around 500 μm thick, which is much thicker than the membranes utilized in this system. To prove that in our system, NO loss during sampling is negligible, we used controllable NO releasing polymer SNAP-PDMS to release NO with a constant rate. NO rate was

measured directly and across the membrane. Result shows that no statistic detectable signal loss within the membrane (data not shown). So in our method, we emphasize close measurement, where NO undergoes the least chemical consumption between its generation and being captured by detectors after crossing the thin PDMS layer.

Any extra treatment to cell during measurement (such as stirring, probe placement, sampling chemicals and dyes) may potentially bring about contamination, cell damage, or alter cell behavior. Our method was able to maintain cell sheet integrity and cell growth condition during NO sampling. Cells were also easily treated with stimulants and inhibitors (such as substrates and drugs), and the resultant changes to NO generation were able to be monitored in real-time during the whole experiment. It is clear that NO production from cells depends on a series complex of factors. But it's unclear how much each parameter contributes to this process. If all the cell work to date related to NO generation had the corresponding direct, real-time NO measurement levels to accompany the elegant molecular biology that has been completed in an effort to understand how various factors influence NO production, our level of understanding of the normal and pathological roles NO plays in health and disease would be staggering. By accurately measuring both the dose and timing of NO production in cells and tissues, we will be able to accelerate our understanding of the diverse and sometimes apparently contradictory effects of NO in normal and pathological states.

4. Conclusions

We fabricated CellNO trap, a two-chamber NO measurement device that is capable of quantitatively analyzing the level of NO produced by cells in a continuous, real-time manner. The device design was validated by using NO-releasing polymer (SNAP-PDMS) that generates NO in a highly controllable manner, which allowed the functional characteristics and potential utility of this device to be investigated. The upper chamber of the device was then used to culture RAW267.4 cells and investigate NO production from the cells using different stimuli and inhibitors. NO generated by the cells diffuses through a hydrophobic, gas permeable membrane that serves as the bottom of the culturing dish into a lower chamber that allows NO to be swept to a chemiluminescence detector, thereby quantitating the level of NO produced by cells. This is the first device to be reported that truly achieved real-time cellular NO measurement without disturbing the cells under investigation or deviating from standard cell culturing protocols. This device opens up a huge potential for increasing our understanding the role NO plays in both normal and pathological conditions in a variety of tissues and could potentially accelerate our ability to design NO releasing and generating therapeutic interventions by allowing quantitative understanding of both the dose and temporal aspects of NO production in cells.

Acknowledgments

This work was funded by the National Science Foundation - Division of Materials Research Grant number 1410192.

References

[1] D.D. Thomas, et al., The chemical biology of nitric oxide: implications in cellular signaling, Free Radic. Biol. Med. 45 (1) (2008) 18–31.
[2] G.A. Blaise, et al., Nitric oxide, cell signaling and cell death, Toxicology 208 (2) (2005) 177–192.
[3] C.-Q. Li, G.N. Wogan, Nitric oxide as a modulator of apoptosis, Cancer Lett. 226 (1) (2005) 1–15.
[4] V. Calabrese, et al., Nitric oxide in the central nervous system: neuroprotection versus neurotoxicity, Nat. Rev. Neurosci. 8 (10) (2007) 766–775.
[5] A.S. Vidwans, et al., Analysis of the neuroprotective effects of various nitric oxide donor compounds in murine mixed cortical cell culture, J. Neurochem. **72** (5) (1999) 1843–1852.
[6] L.A. Ridnour, et al., Molecular mechanisms for discrete nitric oxide levels in cancer, Nitric Oxide 19 (2) (2008) 73–76.
[7] M.B. Grisham, D. Jourd'Heuil, D.A. Wink, I. Physiological chemistry of nitric oxide and its metabolites: implications in inflammation, Am. J. Physiol. – Gastrointest. Liver Physiol. 276 (2) (1999) G315–G321.
[8] B. Mellion, et al., Evidence for the inhibitory role of guanosine 3′, 5′-monophosphate, Blood 57 (1981) 5.
[9] M.W. Radomski, R. Palmer, S. Moncada, The anti-aggregating properties of vascular endothelium: interactions between prostacyclin and nitric oxide, Br. J. Pharmacol. 92 (3) (1987) 639.
[10] R. Gifford, et al., Mediation of in vivo glucose sensor inflammatory response via nitric oxide release, J. Biomed. Mater. Res. Part A 75 (4) (2005) 755–766.
[11] B.J. Nablo, A.R. Rothrock, M.H. Schoenfisch, Nitric oxide-releasing sol–gels as antibacterial coatings for orthopedic implants, Biomaterials 26 (8) (2005) 917–924.
[12] J. Umans, R. Levi, Nitric oxide in the regulation of blood flow and arterial pressure, Annu. Rev. Physiol. (1995) 771–790.
[13] S.H. Baek, et al., Augmentation of intrapericardial nitric oxide level by a prolonged-release nitric oxide donor reduces luminal narrowing after porcine coronary angioplasty, Circulation 105 (23) (2002) 2779–2784.
[14] A. Chaux, et al., Perivascular delivery of a nitric oxide donor inhibits neointimal hyperplasia in vein grafts implanted in the arterial circulation, J. Thorac. Cardiovasc. Surg. 115 (3) (1998) 604–614.
[15] M.C. Frost, M.M. Reynolds, M.E. Meyerhoff, Polymers incorporating nitric oxide releasing/generating substances for improved biocompatibility of blood-contacting medical devices, Biomaterials 26 (14) (2005) 1685–1693.
[16] M.M. Reynolds, M.C. Frost, M.E. Meyerhoff, Nitric oxide-releasing hydrophobic polymers: preparation, characterization, and potential biomedical applications, Free Radic. Biol. Med. 37 (7) (2004) 926–936.
[17] L.K. Keefer, Progress toward clinical application of the nitric oxide-releasing diazeniumdiolates 1, Annu. Rev. Pharmacol. Toxicol. 43 (1) (2003) 585–607.
[18] M.C. Frost, et al., In vivo biocompatibility and analytical performance of intravascular amperometric oxygen sensors prepared with improved nitric oxide-releasing silicone rubber coating, Anal. Chem. 4 (23) (2002) 5942–5947.
[19] K.S. Bohl, J.L. West, Nitric oxide-generating polymers reduce platelet adhesion and smooth muscle cell proliferation, Biomaterials 21 (22) (2000) 2273–2278.
[20] H.A. Moynihan, S.M. Roberts, Preparation of some novel S-nitroso compounds as potential slow-release agents of nitric oxide in vivo, J. Chem. Soc. Perkin Trans. 1 (7) (1994) 797–805.
[21] H. Zhang, et al., Nitric oxide releasing silicone rubbers with improved blood compatibility: preparation, characterization, and in vivo evaluation, Biomaterials 23 (6) (2002) 1485–1494.
[22] R.A. Hunter, et al., Inaccuracies of nitric oxide measurement methods in biological media, Anal. Chem. 85 (3) (2013) 1957–1963.
[23] S. Archer, Measurement of nitric oxide in biological models, FASEB J. 7 (2) (1993) 349–360.
[24] Z.H. Taha, Nitric oxide measurements in biological samples, Talanta 61 (1) (2003) 3–10.
[25] D. Yao, A.G. Vlessidis, N.P. Evmiridis, Determination of nitric oxide in biological samples, Microchim. Acta 147 (1–2) (2004) 1–20.
[26] N.S. Bryan, M.B. Grisham, Methods to detect nitric oxide and its metabolites in biological samples, Free Radic. Biol. Med. 43 (5) (2007) 645–657.
[27] F. Bedioui, N. Villeneuve, Electrochemical nitric oxide sensors for biological samples–principle, selected examples and applications, Electroanalysis 15 (1) (2003) 5–18.
[28] B.W. Allen, J. Liu, C.A. Piantadosi, Electrochemical detection of nitric oxide in biological fluids, Methods Enzym. 396 (2005) 68–77.
[29] D. Tsikas, Review Methods of quantitative analysis of the nitric oxide metabolites nitrite and nitrate in human biological fluids, Free Radic. Res. 39 (8) (2005) 797–815.
[30] J.N. Bates, Nitric oxide measurement by chemiluminescence detection, Neuroprotocols 1 (2) (1992) 141–149.
[31] D. Giustarini, et al., Nitrite and nitrate measurement by Griess reagent in human plasma: evaluation of interferences and standardization, Methods Enzym. 440 (2008) 361–380.
[32] J.R. Lancaster, A tutorial on the diffusibility and reactivity of free nitric oxide, Nitric Oxide 1 (1) (1997) 18–30.
[33] J.R. Lancaster, Simulation of the diffusion and reaction of endogenously produced nitric oxide, Proc. Natl. Acad. Sci. 91 (17) (1994) 8137–8141.
[34] M.T. Gladwin, et al., Relative role of heme nitrosylation and β-cysteine 93 nitrosation in the transport and metabolism of nitric oxide by hemoglobin in the human circulation, Proc. Natl. Acad. Sci. 97 (18) (2000) 9943–9948.
[35] B.Y. Owusu, R. Stapley, R.P. Patel, Nitric oxide formation versus scavenging: the red blood cell balancing act, J. Physiol. 590 (20) (2012) 4993–5000.
[36] B.G. Hill, et al., What part of NO don't you understand? Some answers to the cardinal questions in nitric oxide biology, J. Biol. Chem. 285 (26) (2010) 19699–19704.
[37] B.J. Privett, J.H. Shin, M.H. Schoenfisch, Electrochemical nitric oxide sensors for physiological measurements, Chem. Soc. Rev. 39 (6) (2010) 1925–1935.

[38] Y. Lee, et al., Improved planar amperometric nitric oxide sensor based on platinized platinum anode. 2. Direct real-time measurement of NO generated from porcine kidney slices in the presence of l-arginine, l-arginine polymers, and protamine, Anal. Chem. 76 (3) (2004) 545–551.
[39] A. Fontijn, A.J. Sabadell, R.J. Ronco, Homogeneous chemiluminescent measurement of nitric oxide with ozone. Implications for continuous selective monitoring of gaseous air pollutants, Anal. Chem. 42 (6) (1970) 575–579.
[40] A.J. Dunham, R.M. Barkley, R.E. Sievers, Aqueous nitrite ion determination by selective reduction and gas phase nitric oxide chemiluminescence, Anal. Chem. 67 (1) (1995) 220–224.
[41] D.D. Thomas, et al., Hypoxic inducible factor 1α, extracellular signal-regulated kinase, and p53 are regulated by distinct threshold concentrations of nitric oxide, Proc. Natl. Acad. Sci. USA 101 (24) (2004) 8894–8899.
[42] G.E. Romanowicz, M. Nielsen, M.C. Frost, S-Nitroso-N-acetyl-d-penicillamine covalently linked to polydimethylsiloxane (SNAP–PDMS) for use as a controlled photoinitiated nitric oxide release polymer, Sci. Technol. Adv. Mater. 12 (5) (2011) 055007.
[43] M. Starrett, et al., Wireless platform for controlled nitric oxide releasing optical fibers for mediating biological response to implanted devices, Nitric Oxide 27 (4) (2012) 228–234.
[44] H.A. Moynihan, S.M. Roberts, Preparation of some novel S-nitroso compounds as potential slow-release agents of nitric oxide in vivo, J. Chem. Soc., Perkin Trans. 1 7 (7) (1994) 797–805.
[45] K.A. Mowery, M.E. Meyerhoff, The transport of nitric oxide through various polymeric matrices, Polymer 40 (22) (1999) 6203–6207.
[46] H. Lee, et al., Mussel-inspired surface chemistry for multifunctional coatings, Science 318 (5849) (2007) 426.
[47] C. Xu, et al., In vitro study of human vascular endothelial cell function on materials with various surface roughness, J. Biomed. Mater. Res. Part A 71A (1) (2004) 154–161.
[48] M.P. Chin, D.B. Schauer, W.M. Deen, Nitric oxide, oxygen, and superoxide formation and consumption in macrophages and colonic epithelial cells, Chem. Res. Toxicol. 23 (4) (2010) 778–787.
[49] R.S. Lewis, et al., Kinetic analysis of the fate of nitric oxide synthesized by macrophages in vitro. Journal of Biologcal, Chemistry 270 (49) (1995) 29350–29355.
[50] N. Nalwaya, W.M.D. Deen, Nitric oxide, oxygen, and superoxide formation and consumption in macrophage cultures, Chem. Res. Toxicol. 18 (3) (2005) 486–493.
[51] T. Noda, F. Amano, Differences in nitric oxide synthase activity in a macrophage-like cell line, RAW264. 7 cells, treated with lipopolysaccharide (LPS) in the presence or absence of interferon-γ (IFN-γ): possible heterogeneity of iNOS activity, J. Biochem. 121 (1) (1997) 38–46.
[52] S.J. Morris, Regulation of enzymes of the urea cycle and arginine metabolism, Annu. Rev. Nutr. 22 (1) (2002) 87–105.
[53] C. Wang, W.M. Deen, Nitric oxide delivery system for cell culture studies, Ann. Biomed. Eng. 31 (1) (2003) 65–79.